Acta Polytechnica **62**(4):409–417, 2022
https://doi.org/10.14311/AP.2022.62.0409

Published by the Czech Technical University in Prague

PERFORMANCE OF A HYDROMAGNETIC SQUEEZE FILM ON A ROUGH CIRCULAR STEP BEARING: A COMPARISION OF DIFFERENT POROUS STRUCTURES

Jatinkumar V. Adeshara[a], Hardik P. Patel[b,*], Gunamani B. Deheri[c], Rakesh M. Patel[d]

[a] *Vishwakarma Government Engineering College, Chandkheda, Ahmedabad - 382424 Gujarat State, India*
[b] *L. J. Institute of Engineering and Technology, Department of Humanity and Science, Ahmedabad, Gujarat State, India*
[c] *Sardar Patel University, Department of Mathematics, Vallabh Vidyanagar - 388 120 Gujarat State, India*
[d] *Gujarat Arts and Science College, Department of Mathematics, Ahmedabad - 380 006 Gujarat State, India*
[*] corresponding author: hardikanny82@gmail.com

Abstract.

This investigation deals with a comparative analysis of the impact of spongy structure based on the model of Kozeny-Carman and Irmay on a hydromagnetic squeeze film in a rough circular step bearing. Christensen and Tonder's stochastic averaging process has been utilized to determine the role of an arbitrary transverse surface irregularity. The distribution of the pressure in the bearing is obtained by solving the concerned generalised stochastically averaged equation of Reynolds' with appropriate boundary conditions. The outcomes show that increasing values of magnetization results in an augmented load. The impact of the surface irregularity (transverse) has been found to be adverse. In addition, the negative effect of the surface irregularity and porosity can be minimised by the positive impact of magnetization, at least in the case of the globular sphere model of Kozeny-Carman. Furthermore, the lower strength of the magnetic field results in an approximately similar performance for both these models. This study offers the possibility that the Kozeny-Carman model could be deployed in comparison with Irmay's model.

Keywords: Hydromagnetic fluid, squeeze film, circular step bearing, surface irregularity, spongy structure.

1. Introduction

The efficiency of bearings was substantially improved as compared to traditional lubricants. The magnetohydrodynamic squeeze film performance between curved annular plates was inspected by Lin. et al. [1]. Patel & Deheri [2] examined the influence of a magnetic fluid lubricant on a squeeze film in conical plates. It was found that the overall efficiency improved with this bearing system. Of course, the feature of the cone's semi-vertical angle was crucial in enhancing the performance. The approach adopted in the Patel & Deheri investigation [2] has been amended and improved by Vadher et al. [3]. Calculating the negative impact of the surface irregularity (transverse) between rough spongy conical plates of a magnetic-fluid-based squeeze film. They found that in the case of the negative skewed surface irregularity, the already-increased load increased even further.

Andharia & Deheri [4] examined the longitudinal effect of a surface irregularity between conical plates on the magnetic-fluid-dependent squeeze film. In relation to the surface irregularity (transverse), the squeeze film associated with the surface irregularity increased the load for a cylindrical squeeze film, Lin [5] developed a ferrofluid lubrication equation that takes into account convective fluid inertia forces for a circular disc application. Compared to the non-inertia non-ferrofluid case, a longer elapsed period was found. The product of a squeeze film based on magnetic fluid between rough (longitudinally) elliptical plates has already been considered by Andharia & Deheri [6]. It was noted that due to the combination of the squeeze film and the negative skewed surface irregularity, the load increased significantly due to the magnetisation. The Shliomis-model-based ferrofluid lubrication of a squeeze film was discussed by Patel & Deheri [7] for rotating rough (transversely) curved circular plates. Such a type of bearing structure allows a certain amount of load even though there is no flow of a typical lubricant. Very recently, Patel et al. [8]) investigated a squeeze film behaviour of different spongy structures on rough conical plates. The Kozeny-Carman model is preferred over the Irmay's model for spongy structure in the case of a surface irregularity (transverse). Hydromagnetic squeeze film in rough truncated conical plates, using the Kozeny-Carman-model-based spongy structure, was discussed by Adeshara et al. [9].

A new kind of bearing is introduced by Robert Goraj [10], where the thickness of the lubricant is also used as an electromagnetic system air gap. Here, under hydrodynamic, electromagnetic, and gravity stresses, a new

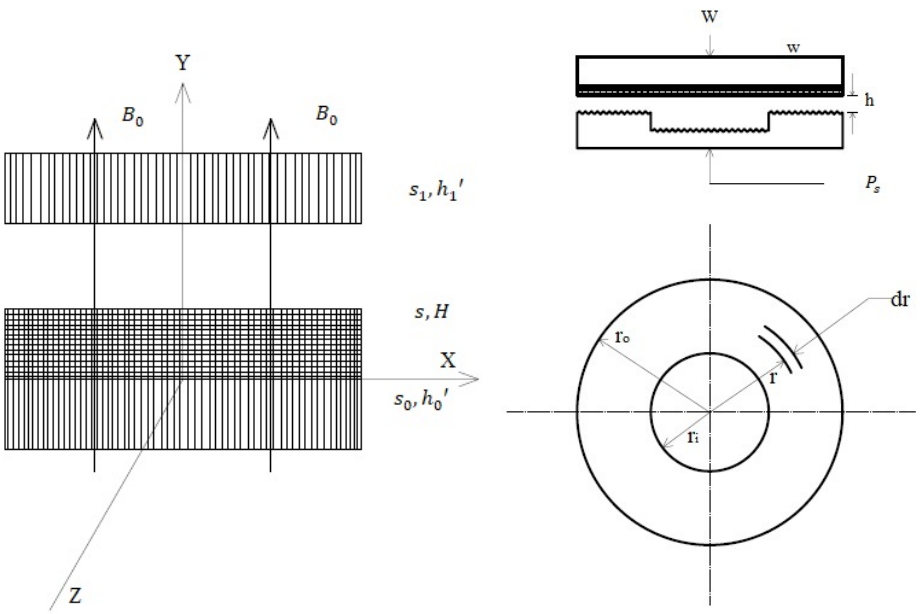

FIGURE 1. The bearing system design and specification are given.

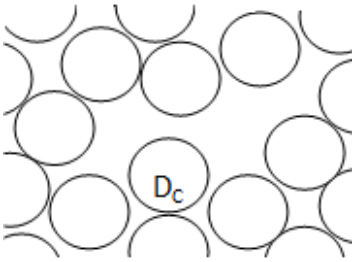

FIGURE 2. Configuration of spongy sheets given by Kozeny-Carman.

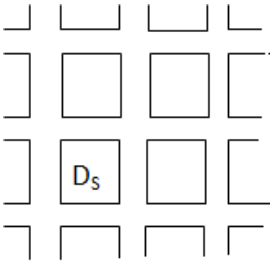

FIGURE 3. Configuration of spongy sheets provided by Irmay.

governing equation system defining steady loci of such an electromagnetically supported short hydrodynamic plain journal bearing is obtained and solved. Lu et al. [11] develops an analytic model to predict the static properties of a new hydrodynamic–rolling hybrid bearing. The findings demonstrate that the hydrodynamic–rolling hybrid bearing working states are split into two separate phases by a transition speed at which the hydrodynamics and contact models are separated. The impact of surface roughness and micropolar lubricant between two elliptical plates under the application of an external transverse magnetic field was analysed by Halambi et al. [12]. Younes et al. [13] have presented several strategies for increasing the thermal conductivity of these fluids by suspending nano/micro-sized particle materials in them. Patel and Deheri [14] discussed the influence of viscosity variation on ferrofluid-based long bearing. In this article, it is observed that the increased load carrying capacity, due to the magnetization, is not significantly affected by viscosity variation.

In this article, it has been sought to study and analyse the performance of hydromagnetic squeeze film on a rough circular step bearing with inclusion of two different porous structures: Kozeny-Carman and Irmay's model. Furthermore, the effect of transverse roughness on the bearing's performance is also discussed.

2. ANALYSIS

The lower plate with a porous facing is assumed to be fixed while the upper plate moves along its normal towards the lower plate. The plates are considered electrically conductive and the clearance space between them is filled by an electrically conducting lubricant. A uniform transverse magnetic field is applied between the plates. The flow in the porous medium obeys the modified form of Darcy's law.

As shown in Figure 1, here, bearings are not in direct contact and the load is applied on the bearings. The load w is carried within the pocket and surface by the fluid. The fluid flows in a radial direction. Following the analyses of Majumdar [15], and Patel, Deheri & Vadher [8], one finds that the Reynolds-type equation

for the pressure induced flow in a circular-step bearing is

$$Q = -\frac{2\pi r \frac{\mathrm{d}p}{\mathrm{d}r}\left[\frac{2A}{M^3}\left[\frac{M}{2} - \tanh\frac{M}{2}\right] + \frac{\psi l_1 A}{c^2}\right]\left[\frac{\phi_0 + \phi_1 + 1}{\phi_0 + \phi_1 + \left(\tanh\frac{M}{2}\right)/\left(\frac{M}{2}\right)}\right]}{12\mu}, \tag{1}$$

where

$$A = h^3 + 3h^2\alpha + 3h\left(\alpha^2 + \sigma^2\right) + \varepsilon + 3\sigma^2\alpha + \alpha^3. \tag{2}$$

2.1. Case – I (A globular sphere model as displayed in Figure 2)

This model includes the globular sphere to fill in the spongy content of particles. The mean particle size is D_c. The permeability of the spongy region was found to be

$$\psi = \frac{D_c^2 e_1^3}{180\left(1 - e_1\right)^2}, \tag{3}$$

where e_1 is the porosity. Integrate the above equation (1) with respect to the boundary condition. Using Reynolds' boundary condition

$$\begin{aligned} r = r_0, \quad p = 0, \\ r = r_i, \quad p = p_s. \end{aligned} \tag{4}$$

The leading film pressure equation p is given by the

$$p = p_s \frac{\ln\left(\frac{r}{r_o}\right)}{\ln\left(\frac{r_i}{r_o}\right)}, \tag{5}$$

where in

$$p_s = \frac{6\ln\left(\frac{r_o}{r_i}\right)}{\pi\left[\frac{2A}{M^3}\left[\frac{M}{2} - \tanh\frac{M}{2}\right] + \frac{D_c^2 e_1^3 l_1 A}{180\left(1 - e_1\right)^2 c^2}\right]\left[\frac{\phi_0 + \phi_1 + 1}{\phi_0 + \phi_1 + \left(\tanh\frac{M}{2}\right)/\left(\frac{M}{2}\right)}\right]}. \tag{6}$$

Here non-dimensional equation

$$P_s^* = \frac{6\ln\left(\frac{1}{k}\right)}{\pi\left[\frac{2B}{M^3}\left[\frac{M}{2} - \tanh\frac{M}{2}\right] + \frac{\overline{\psi} B e_1^3}{15\left(1 - e_1\right)^2 c^2}\right]\left[\frac{\phi_0 + \phi_1 + 1}{\phi_0 + \phi_1 + \left(\tanh\frac{M}{2}\right)/\left(\frac{M}{2}\right)}\right]}. \tag{7}$$

Introducing the non-dimensional quantities

$$\begin{aligned} B = 1 + 3\alpha^* + 3\left(\alpha^{*2} + \sigma^{*2}\right) + \varepsilon^* + 3\sigma^{*2}\alpha^* + \alpha^{*3}, \\ \alpha^* = \left(\frac{\alpha}{h}\right), \quad \sigma^* = \left(\frac{\sigma}{h}\right), \quad \varepsilon^* = \left(\frac{\varepsilon}{h^3}\right), \quad k = \left(\frac{r_i}{r_o}\right), \quad \overline{\psi} = \frac{D_c^2 l_1}{h^3}. \end{aligned} \tag{8}$$

By integrating the pressure that takes the dimensionless form, the load w is computed.

$$W = \frac{P_s^*\left(1 - k^2\right)}{2\ln\left(\frac{1}{k}\right)}. \tag{9}$$

2.2. Case – II (model with capillary fissures as revealed in Figure 3)

This model deals with three sets of mutually orthogonal fissures (mean solid size D_s). Irmay [16] assumed no loss of hydraulic gradient at the junction and derived the expression for the spongy structure parameter as

$$\psi = \frac{(1 - m)^{2/3} D_s^2}{12m}, \tag{10}$$

where $m = 1 - e_1$, e_1 being the porosity. The governing equation for the film pressure p is given by

$$p = p_s \frac{\ln\left(\frac{r}{r_o}\right)}{\ln\left(\frac{r_i}{r_o}\right)}, \tag{11}$$

$$p_s = \frac{6\ln\left(\frac{r_o}{r_i}\right)}{\pi\left[\frac{2A}{M^3}\left[\frac{M}{2} - \tanh\frac{M}{2}\right] + \frac{(1-m)^{2/3}D_s^2 l_1 A}{12mc^2}\right]\left[\frac{\phi_0+\phi_1+1}{\phi_0+\phi_1+\left(\tanh\frac{M}{2}\right)/\left(\frac{M}{2}\right)}\right]}. \tag{12}$$

Here, non-dimensional equation

$$P_s^* = \frac{6\ln\left(\frac{1}{k}\right)}{\pi\left[\frac{2B}{M^3}\left[\frac{M}{2} - \tanh\frac{M}{2}\right] + \frac{\overline{\psi}B(1-m)^{2/3}}{mc^2}\right]\left[\frac{\phi_0+\phi_1+1}{\phi_0+\phi_1+\left(\tanh\frac{M}{2}\right)/\left(\frac{M}{2}\right)}\right]}. \tag{13}$$

Introducing the non-dimensional quantities

$$B = 1 + 3\alpha^* + 3\left(\alpha^{*2} + \sigma^{*2}\right) + \varepsilon^* + 3\sigma^{*2}\alpha^* + \alpha^{*3}, \tag{14}$$

where

$$\overline{\psi} = \frac{D_s^2 l_1}{h^3}.$$

The load w is calculated by integrating the pressure, which takes the dimensionless form

$$W = \frac{P_s^*\left(1-k^2\right)}{2\ln\left(\frac{1}{k}\right)}. \tag{15}$$

3. Results and discussions

In the absence of porous structures, the current study reduces to the deliberation of hydromagnetic squeeze film in rough circular step bearing. Further, for smooth bearing surfaces, this analysis comes down to the discussion of circular step bearing (Majumdar [15]), when there is no magnetization. However, because of porous structures, there is an additional degree of freedom from a bearing design point of view. Equations (7) and (13) describe the dimensionless pressure profile, while equations (9) and (15) govern the non-dimensional load. These expressions clearly suggest that the load $W \propto P_s^*$ and

$$p_s = \frac{Q}{\pi\left[\frac{2A}{M^3}\left[\frac{M}{2} - \tanh\frac{M}{2}\right] + \frac{\psi l_1 A}{c^2}\right]\left[\frac{\phi_0+\phi_1+l}{\phi_0+\phi_1+\left(\tanh\frac{M}{2}\right)/\left(\frac{M}{2}\right)}\right]}.$$

This means that the load increases with a constant flow rate as the stochastically averaged squeeze film decreases in thickness. The bearing is thus self-compensating, provided that the flow rate is assumed to be constant. Equations (7) and (13), (9) and (15) indicate that the effect of conductivity parameters on the pressure distribution and load is determined by

$$\frac{\phi_0+\phi_1+\left(\tanh\frac{M}{2}\right)/\left(\frac{M}{2}\right)}{\phi_0+\phi_1+1},$$

which turns to

$$\frac{\phi_0+\phi_1}{\phi_0+\phi_1+1},$$

for big values of M, because as $\tanh M \cong 1$ and $(2/M) \cong 0$. Furthermore, it is observed that the pressure and load rise with growths in $\phi_0 + \phi_1$ because both the functions are growing functions of $\phi_0 + \phi_1$.

Figures 4, 5, 8, 9, 12, 13, 16, 17, 20, 21, 24, 26 deal with the pattern of the load with respect to different parameters for Kozeny-Carman's globular sphere model, Figures 6, 7, 10, 11, 14, 15, 18, 19, 22, 23, 25, 27 deal with the variance of the load in relation to Irmay's model of capillary fissures.

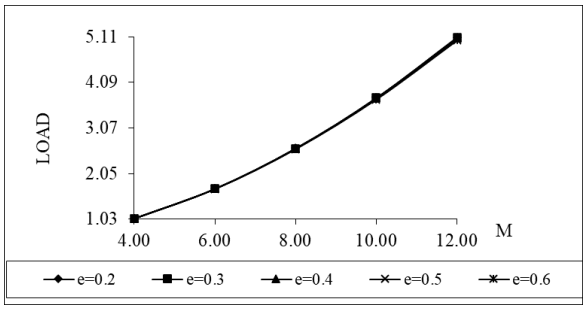

FIGURE 4. Profile of load with M & e.

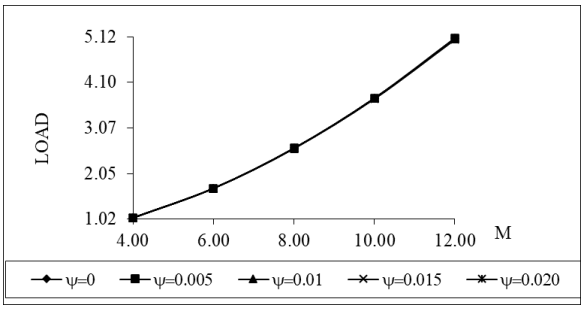

FIGURE 5. Data of load with M & ψ.

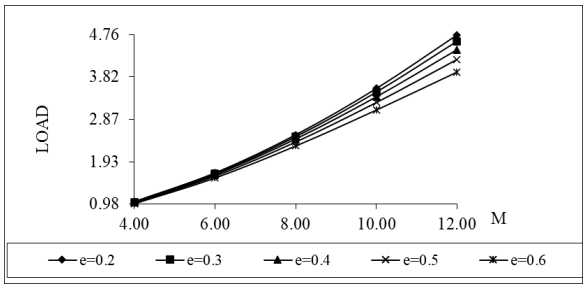

FIGURE 6. Data of load with M & e.

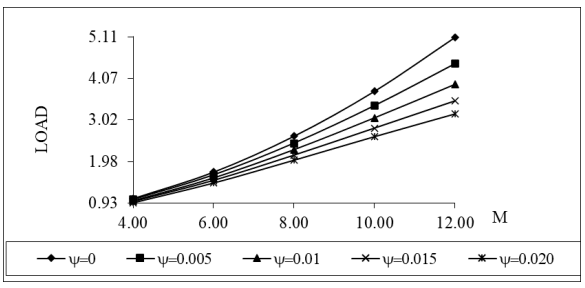

FIGURE 7. Change of load with M & ψ.

Increased magnetization parameters will then contribute to an increased load as can be seen in Figures 4 and 5 and Figures 6 and 7, it can be noted that the rate of the increase in the load is comparatively greater in Kozen-Carman's globular sphere model. However, in the case of the globular sphere model, the impact of spongy structure parameters and porosity on the variation of load with regard to magnetization is negligible to some degree. For both models, the load increases sharply.

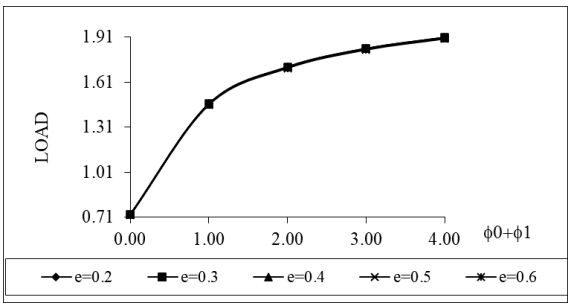

FIGURE 8. Change of load with $\phi_0 + \phi_1$ & e.

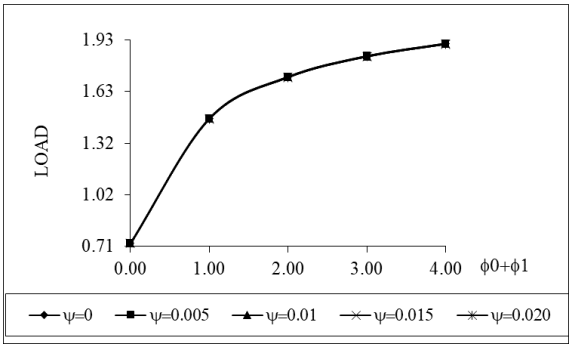

FIGURE 9. Profile of load with $\phi_0 + \phi_1$ & ψ.

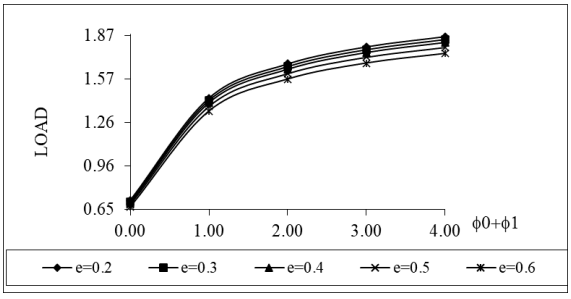

FIGURE 10. Data of load with $\phi_0 + \phi_1$ & e.

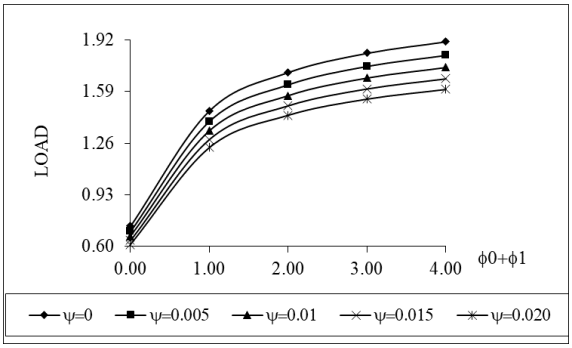

FIGURE 11. Change of load with $\phi_0 + \phi_1$ & ψ.

The effect of $\phi_0 + \phi_1$ on the distribution of the load with respect to the Kozeny-Carman model is shown in Figures 8 and 9, while the profile of the load for the Irmay model is given in Figures 10 and 11. The rate

of the increase in the load is comparatively higher in Kozeny-Carman's globular sphere model as compared to Irmay's capillary fissures model.

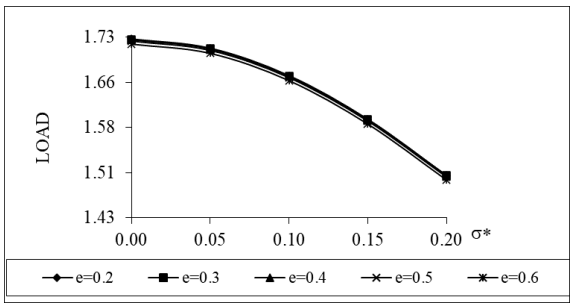

FIGURE 12. Variation of load with σ^* & e.

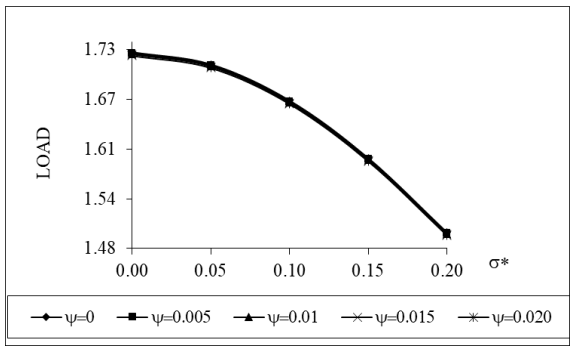

FIGURE 13. Data of load with σ^* & ψ.

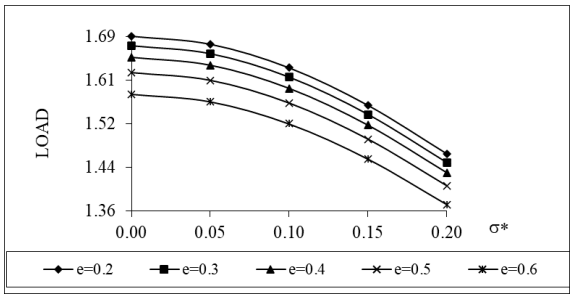

FIGURE 14. Data of load with σ^* & e.

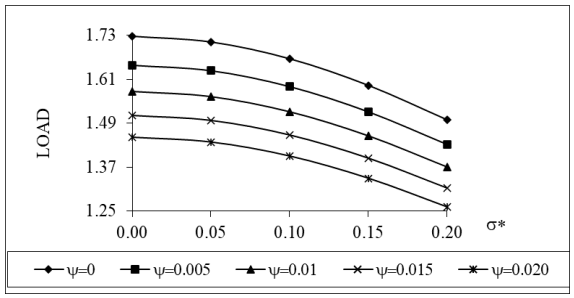

FIGURE 15. Profile of load with σ^* & ψ.

Figures 12 and 13 provide the squeeze film effect on the distribution of the load with respect to the Kozeny-Carman's model and Irmay model in Figures 14 and 15. It can be seen that an increase in the values of squeeze film results in an increased load and, consequently, adversely affects the squeeze film performance. As can be seen from Figures 12 and 13, for the Kozeny-Carman model, the effect of the spongy structure and porosity on the variance of the load carrying capacity with regard to the squeeze film is marginal, but in the Irmay model, it is negligible.

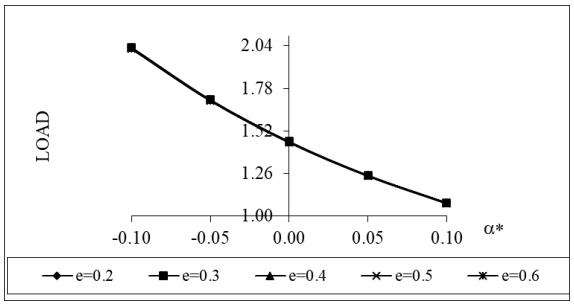

FIGURE 16. Change of load with α^* & e.

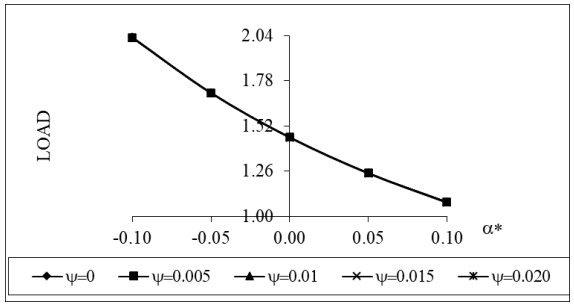

FIGURE 17. Variation of load with α^* & ψ.

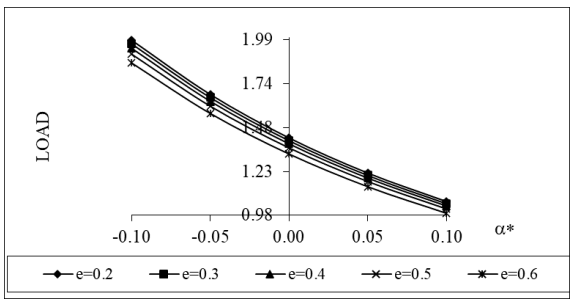

FIGURE 18. Trend of load with α^* & e.

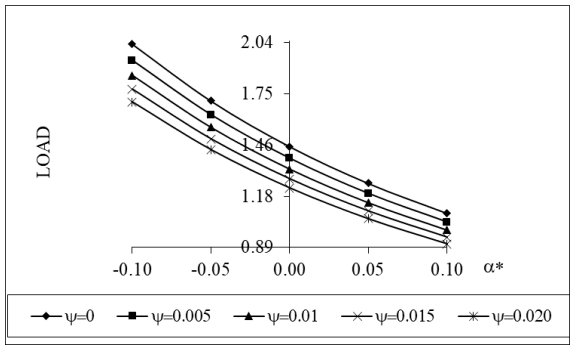

FIGURE 19. Profile of load with α^* & ψ.

It is found that the load bearing capacity decreases due to the positive variance. The opposite of this trend is visible in the case of the negative variance for both models (Kozeny-Carman and Irmay). It is important to note that the influence of the spongy structure parameter on the variation of the load remains negligible for the Kozeny-Carman model with respect to variance. (Figures 16 and 17) and Irmay's model (Figures 18 and 19).

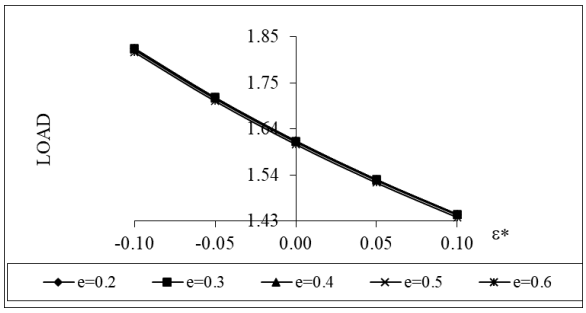

FIGURE 20. Data of load with ε^* & e.

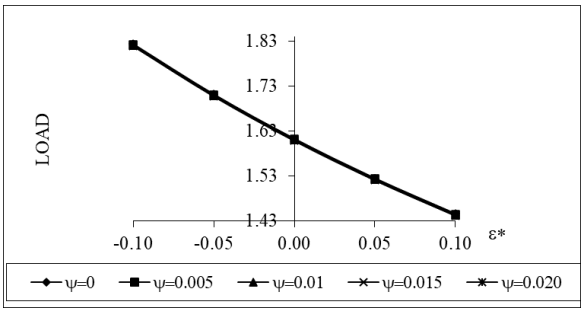

FIGURE 21. Change of load with ε^* & ψ.

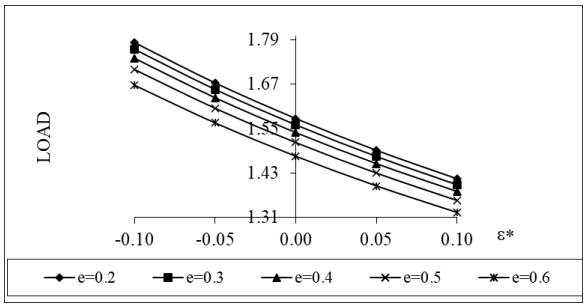

FIGURE 22. Variation of load with ε^* & e.

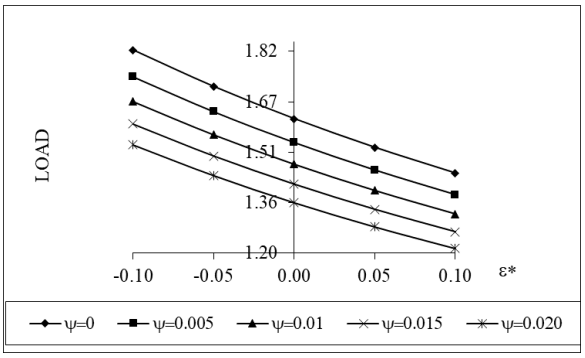

FIGURE 23. Profile of load with ε^* & ψ.

The effect of skewness for the Kozeny-Carman model and Irmay's model is presented in Figures 20 and 21 and Figures 22 and 23, respectively. The increased load due to variance (-ve) gets further increased as a result of the negatively skewed surface irregularity. Here, the effect of the spongy structure parameter and porosity is also negligible in the case of Kozeny-Carman model, while a better performance can be seen in the case of Irmay's model.

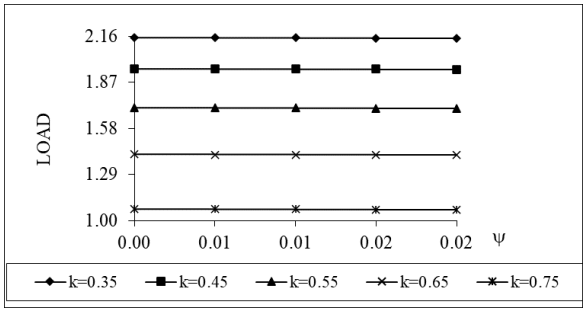

FIGURE 24. Profile of load with ψ & k.

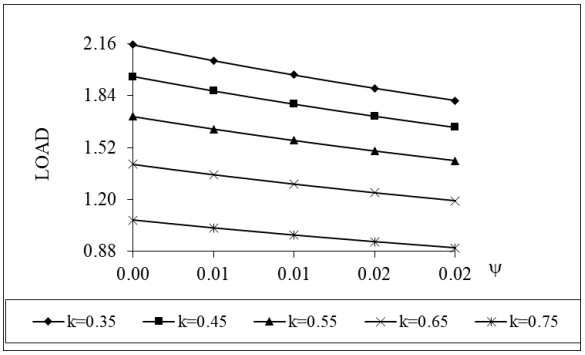

FIGURE 25. Trend of load with ψ & k.

The combined effect of the spongy structure parameter and radii ratio (k) appears to be adverse, which can be seen from Figures 24 and 25. However, at the outset, the decrease in load is more profound in the case of Irmay's model.

The effect of porosity and redii ratio is presented in Figure 26 for Kozeny-Carman model and Figure 27 for Irmay's model. For Irmay's model, only an increase can be seen, however, that is not the case for Kozeny-Carman model.

A comparison of both models is presented. From Table 1, one can see that Kozeny-Carman model provides a better performance as compared to Irmay's model with regards to the transverse roughness.

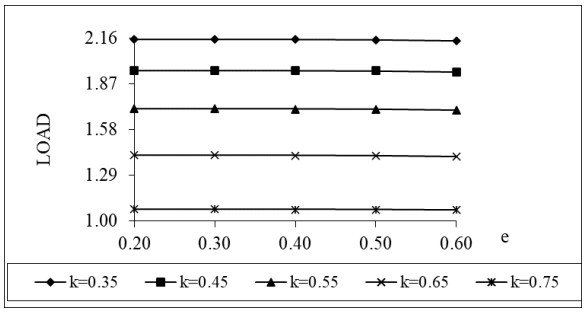

FIGURE 26. Variation of load with e & k.

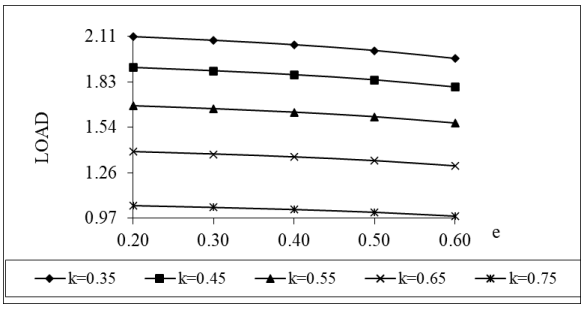

FIGURE 27. Change of load with e & k.

		Kozeny-Carman's globular sphere model		Irmay's model of capillary fissures	
Sr. No	Graph	Minimum	Maximum	Minimum	Maximum
1	$M \to e$	1.04178748	5.10051255	0.99169035	4.75745642
2	$M \to \psi$	1.04311200	5.10122332	0.94204858	5.10122332
3	$\phi_0 + \phi_1 \to e$	0.72690126	1.90743812	0.66815659	1.86550029
4	$\phi_0 + \phi_1 \to \psi$	0.72851122	1.90752098	0.61379908	1.90752098
5	$\sigma^* \to e$	1.49304632	1.72660919	1.37238548	1.68864716
6	$\sigma^* \to \psi$	1.49635317	1.72668420	1.26073582	1.72668420
7	$\alpha^* \to e$	1.07736948	2.03056534	0.99030164	1.98592038
8	$\alpha^* \to \psi$	1.07975567	2.03065355	0.90973620	2.03065355
9	$\varepsilon^* \to e$	1.43886631	1.82372390	1.32258403	1.78362666
10	$\varepsilon^* \to \psi$	1.44205315	1.82380313	1.21498594	1.82380313
11	$\psi \to k$	1.07109072	2.15361105	0.90243565	2.15361105
12	$e \to k$	1.06872368	2.15351750	0.98235456	2.10616926

TABLE 1. A comparison of both models.

4. CONCLUSION

This analysis demonstrates that the Kozeny-Carman model is a better choice for this type of bearing design. Furthermore, this research shows that the surface irregularity aspect must be carefully considered while designing the bearing systems, even if the required magnetic strength is employed. This can play a vital role in improving the overall performance in the case of Irmay's model. In addition, in the absence of flow, the bearing system supports some load for these two models, which never occurs for traditional lubricants and this load is comparatively higher in the case of Kozeny-Carman model.

ACKNOWLEDGEMENTS

The authors would like to thank the reviewers for their valuable remarks and suggestions for the overall improvement of the presentation and organization of the manuscript.

LIST OF SYMBOLS

R Radial coordinate
r_o Outer radius
r_i Inner radius
K $= \frac{r_i}{r_o}$ – Radii ratio
H Film thickness of lubricant
S Lubricant's electrical conductivity
μ Lubricant's viscosity
B_o Uniform transverse magnetic field applied between the plates
M $= B_0 h \left(\frac{s}{\mu}\right)^{1/2}$ – Hartmann Number
p_s Supply Pressure
Q Flow rate
P_s^* Dimensionless supply pressure

P Lubricant pressure
P^* Non-dimensional pressure
W Dimensionless L.C.C
h_0 Lower plate's surface width
h_1 Upper plate's surface width
s_0 Lower surface's electrical conductivity
s_1 Upper surface's electrical conductivity
$\phi_0(h) = \frac{s_0 h_0'}{sh}$ – Electrical permeability of lower surface
$\phi_1(h) = \frac{s_1 h_1'}{sh}$ – Electrical permeability of upper surface
σ^* Non-dimensional S.F.
α^* Dimensionless variance
ε^* Non dimensional skewness
ψ Spongy structure of the spongy region
e_1 Porosity
l_1 Thickness of spongy facing

References

[1] J.-R. Lin, R.-F. Lu, W.-H. Liao. Analysis of magneto-hydrodynamic squeeze film characteristics between curved annular plates. *Industrial Lubrication and Tribology* **56**(5):300–305, 2004. https://doi.org/10.1108/00368790410550714.

[2] R. M. Patel, G. Deheri. Magnetic fluid based squeeze film between porous conical plates. *Industrial Lubrication and Tribology* **59**(3):143–147, 2007. https://doi.org/10.1108/00368790710746110.

[3] P. Vadher, G. Deheri, R. Patel. Performance of hydromagnetic squeeze films between conducting porous rough conical plates. *Meccanica* **45**(6):767–783, 2010. https://doi.org/10.1007/s11012-010-9279-y.

[4] P. I. Andharia, G. Deheri. Longitudinal roughness effect on magnetic fluid-based squeeze film between conical plates. *Industrial Lubrication and Tribology* **62**(5):285–291, 2010. https://doi.org/10.1108/00368791011064446.

[5] J.-R. Lin. Derivation of ferrofluid lubrication equation of cylindrical squeeze films with convective fluid inertia forces and application to circular disks. *Tribology International* **49**:110–115, 2012. https://doi.org/10.1016/j.triboint.2011.11.006.

[6] P. Andharia, G. Deheri. Performance of magnetic-fluid-based squeeze film between longitudinally rough elliptical plates. *International Scholarly Research Notices* **2013**:482604, 2013. https://doi.org/10.5402/2013/482604.

[7] J. R. Patel, G. Deheri. Shliomis model based magnetic fluid lubrication of a squeeze film in rotating rough curved circular plates. *Caribbean Journal of Sciences and Technology (CJST)* **1**:138–150, 2013.

[8] R. M. Patel, G. Deheri, P. Vahder. Hydromagnetic rough porous circular step bearing. *Eastern Academic Journal* **3**:71–87, 2015.

[9] J. Adeshara, H. Patel, G. Deheri. Theoretical study of hydromagnetic S.F. rough truncated conical plates with Kozeny-Carman model based spongy structure. *Proceeding on Engineering sciences* **2**(4):389–400, 2020. https://doi.org/10.24874/PES0204.006.

[10] R. Goraj. Theoretical study on a novel electromagnetically supported hydrodynamic bearing under static loads. *Tribology International* **119**:775–785, 2018. https://doi.org/10.1016/j.triboint.2017.09.021.

[11] D. Lu, W. Zhao, B. Lu, J. Zhang. Static characteristics of a new hydrodynamic–rolling hybrid bearing. *Tribology International* **48**:87–92, 2012. https://doi.org/10.1016/j.triboint.2011.11.010.

[12] B. Halambi, B. N. Hanumagowda. Micropolar squeeze film lubrication analysis between rough porous elliptical plates and surface roughness effects under the MHD. *Ilkogretim Online* **20**(4):307–319, 2021. https://doi.org/10.17051/ilkonline.2021.04.33.

[13] Y. Menni, A. J. Chamkha, A. Azzi. Nanofluid flow in complex geometries – A review. *Journal of Nanofluids* **8**(5):893–916, 2019. https://doi.org/10.1166/jon.2019.1663.

[14] J. Patel, G. Deheri. Influence of viscosity variation on ferrofluid based long bearing. *Reports in Mechanical Engineering* **3**(1):37–45, 2022. https://doi.org/10.31181/rme200103037j.

[15] B. C. Majumdar. *Introduction to tribology of bearings*. AH Wheeler & Company, India, 1986.

[16] S. Irmay. Flow of liquid through cracked media. *Bulletin of the Research Council of Israel* **5**(1):84, 1955.